RSC Advances

PAPER

View Article Online
View Journal | View Issue

Cite this: *RSC Adv.*, 2021, **11**, 38523

Enhanced photocatalytic hydrogen production of MoS_2 sheet/carbon nanofiber using rapid electron transport of Mo^{6+} and carbon nanofiber†

Jianfeng Qiu,[ab] Jiaqi Pan,[ac] Shunhang Wei,[b] Qifeng Liang,[b] Yawei Wang,[d] Rong Wu[e] and Chaorong Li*[ac]

Received 16th September 2021
Accepted 10th November 2021

DOI: 10.1039/d1ra06938a

rsc.li/rsc-advances

Normal MoS_2 exhibits a low photocatalytic performance for H_2 production owing to the deficiency of the active sites and the poor electrical conductance. In this work, MoS_2 anchored on the surface of the carbon nanofibers was designed to enhance the activity of the exposed edge and the electrical conductivity at the same time. The oxidation of the surface Mo atoms increases the activity of the exposed edge of the MoS_2. The introduction of carbon nanofibers facilitates the effective transportation of the electron–hole pairs by enhancing the electrical conductivity. As a result, the introduction of carbon nanofibers and Mo^{6+} can facilitate the electron–hole pair separation to enhance the photocatalytic hydrogen evolution reaction (HER) performance (to eight fold more than normal MoS_2).

Introduction

Owing to being clean, cheap and sustainable, H_2 evolution using photocatalytic water splitting is regarded as a promising technology to convert solar energy.[1–4] In recent decades, a large number of semiconductor photocatalysts have been developed for photocatalytic hydrogen evolution, for example, metal oxides,[5,6] sulfides,[7–10] and oxynitrides.[11,12] Among these, MoS_2, a typical two-dimensional (2D) sulfide, has attracted considerable attention owing to its suitable band gap potential and sufficient hydrogen evolution reaction (HER) active sites.[13–15] However, restricted by the high photo-generated charge carrier recombination,[16] the photocatalytic HER performance of single MoS_2 can barely meet the needs of actual applications. Thus, improving the photo-generated charge carrier separation is the most significant issue for this system.[17] Also, the increased HER active sites and dispersibility are important for further ameliorating the HER performance.[18,19]

As reported, the edges S atoms are regarded as efficient active sites for the HER,[13] and significant efforts have been made to expose more efficient edge S atoms active sites. For example, Li *et al.* have prepared N-doped MoS_2 nanosheets with an enhanced HER performance,[20] Kong *et al.* reported vertically aligned layers of crystalline MoS_2 with a remarkable HER performance,[21] and other specific MoS_2 nanostructures, including nanosheets, nanorods, nanotubes, and so on, have been reported previously.[22–24] However, the HER performance is expected to improve further, especially for promoting the charge carrier separation.[25] As reported, Mo^{6+}, with unique redox properties, was found to play a significant role in the photocatalytic reactions.[26,27] Therefore, introducing Mo^{6+} into MoS_2 may effectively improve the active sites of the Mo edge. On the other hand, rapid transportation of the photo-generated electron is also an effective method for restraining photo-generated charge carrier recombination,[28] therefore, a series of co-catalyst or metallic carriers have been reported as promising candidates, such as NiS_2, MoC_2 or CoS,[29–31] and so forth. Currently, highly carbonated carbon nanofibers,[32] with a high conductivity, low cost, and which are environmentally friendly, are a hot topic of research. In particular, the unique electronic structure of the carbon fibers can maintain a good physical–chemical stability during the rapid HER process and charge carrier transportation.[33–35]

Additionally, the dispersibility is another important factor for photocatalysts, as owing to the large specific surface areas and high surface activity, the nano-catalysts can easily aggregate,[36] leading to inactivation of the nano-catalyst, decreasing the catalytic activity. Therefore, highly dispersive and stable carriers are regarded as having indispensable properties for a highly photocatalytically active systems.[37] Herein, carbon nano-fibers, prepared using the electrospinning–carbonization method,[38] were fabricated and possess both toughness and dispersibility. These properties can provide sufficient specific

[a]*College of Textile Science and Engineering, Zhejiang Sci-Tech University, Hangzhou, 310018, PR China. E-mail: crli@zstu.edu.cn*

[b]*Department of Physics, Shaoxing University, Shaoxing 312000, PR China*

[c]*Key Laboratory of Optical Field Manipulation of Zhejiang Province, Department of Physics, Zhejiang Sci-Tech University, Hangzhou 310018, P. R. China*

[d]*School of Chemistry and Chemical Engineering, Jiujiang University, Jiujiang 332005, PR China*

[e]*School of Physics Science and Technology, Xinjiang University, Urumqi 830000, PR China*

† Electronic supplementary information (ESI) available. See DOI: 10.1039/d1ra06938a

surface areas for MoS_2 deposition and enough dispersibility to prevent aggregation,[33] and are reported to be an ideal carrier.[39,40] Furthermore, this fiber system can be directly recycled from the reaction solution, these properties can decrease the cost, increasing the competitiveness.[41]

In this work, we report the growth of MoS_2 (MS)/carbon nanofibers (CNF) using the electrospinning–carbonization method. Herein, the activity of the MS can be improved by changing the surface valence state (Mo^{6+}), and carbon nanofibers can enhance the electron transportation to restrain the charge carrier recombination and increase the dispersibility. As revealed, the photocatalytic HER activity of the as-prepared MS/CNF exhibits a significantly enhancement of about eight fold upon introduction of the carbon nanofibers.

Experimental

Chemicals

Polyacrylonitrile (PAN; M_w = 150 000; J&K Scientific), *N*,*N*-dimethylformamide (DMF; AR; Aladdin), molybdenum sulfide (MoS_2; 99.5% metals basis; Aladdin), triethanolamine (AR; Aladdin), and absolute ethanol (AR; Aladdin).

Preparation

Polyacrylonitrile (1 g) was added into DMF (10 mL) solution and magnetically stirred for 10 h. MoS_2 (0.2 g) was added into the obtained transparent solution and stirring was continued for 24 h to form a homogenous solution for electrospinning. The obtained homogenous solution was fed into a syringe pump with a 17 kV voltage source. The distance between the needle tip and the collector was 15 cm. The feeding rate of the solution in the syringe was controlled at 1.0 mL h^{-1}. The collected products were calcined at 230 °C in air for 3 h and then calcined at 800 °C in nitrogen for 2 h. A schematic illustration is shown in Fig. 1.

Characterization

The crystalline phases were characterized using X-ray powder diffractometry (XRD, Empyrean). The morphology of the samples was obtained using field emission scanning electron microscopy (FESEM, SIGMA 300) and high-resolution transmission electron microscopy (HRTEM, JEM-2100 F). The elemental chemical states of the samples were examined using X-ray photoelectron spectroscopy (XPS, Thermo ESCALAB250). UV-vis diffuse reflection spectra (DRS) were obtained using a UV-3600 plus spectrophotometer (Shimadzu). The photoluminescence (PL) spectra were measured using a fluorescence spectrophotometer (Hitachi F-7000) with an excitation wavelength of 350 nm. The electrochemical impedance spectroscopy was measured using a CHI 660 electrochemical workstation in a conventional three electrode system.

Photocatalytic activity measurements

Experiments were carried out in a top irradiation-type glass reactor connected to a gas-closed circulation and evacuation system (Labsolar 6A, Perfect Light, China). A 300 W xenon lamp (PLX-SXE300, Perfect Light) was used as a light source. In a typical measurement, 50 mg of the catalyst was suspended in 100 mL of a 10 vol% aqueous solution of triethanolamine (sacrificial reagent). The H_2 produced in the reactor was analyzed using an online gas chromatograph (GC7806, shiweipx, China).

Results and discussion

The XRD and Raman spectra results (Fig. 2 and S1†) show that the MoS_2 (represented by MS) retains the original structure after high temperature carbonization and deposition around the carbon nanofibers (represented as CNF). It should be noted that the diffraction peaks exhibit an obvious broadening, which indicates that the nanocrystal size of the MS decreases after deposition around the carbon nanofibers.[42] The morphologies of MS and MSCNF were characterized using FESEM and HRTEM. As shown, the normal MoS_2 (Fig. 3a) is a typical bulk sample, and the carbon nanofiber (Fig. 3b) with a diameter of approximately 200 nm is smooth and uniform. Significantly, with the formation of the MoS_2/carbon nanofibers, the size of the MoS_2 nanosheets shows an obvious decrease (Fig. 3c), which is beneficial for the HER performance and corresponds to the XRD results. The HRTEM image of MSCNF (Fig. 3e and f) shows that the 0.27 nm lattice spacing corresponds to the (100) facets of the MS, which can further confirm the deposition of MS around the CNF.

X-ray photoelectron spectroscopy (XPS) analysis was used to investigate the surface chemical states of MS and MSCNF, and is shown in Fig. 4a and b. As revealed, the binding energies of Mo $3d_{3/2}$ and Mo $3d_{5/2}$ in the MS located at 232.94 and 229.79 eV

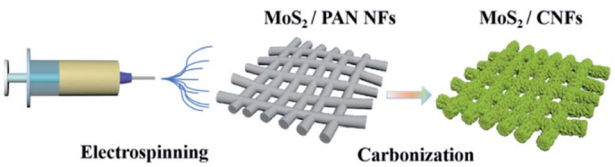

Fig. 1 Schematic illustration of the MSCNF synthetic process.

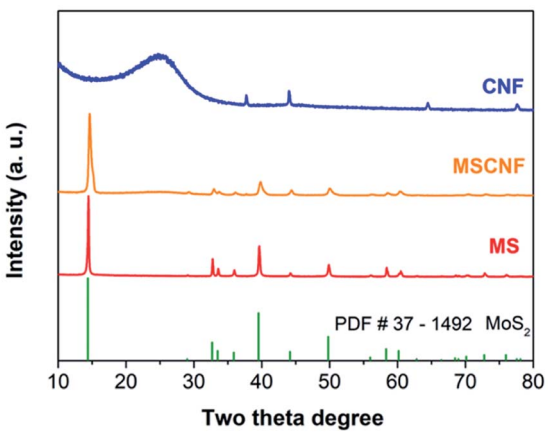

Fig. 2 XRD patterns of the samples.

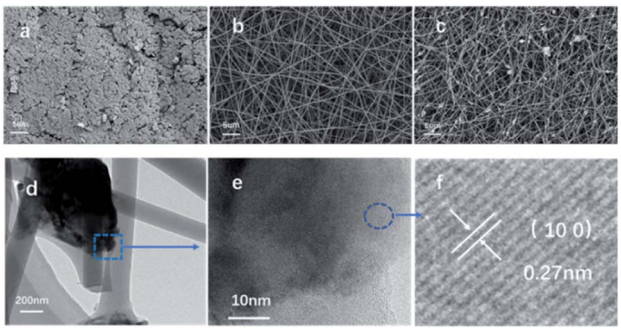

Fig. 3 SEM image of MS (a), CNF (b) and MSCNF (c); and the HRTEM image of MSCNF (d)–(f).

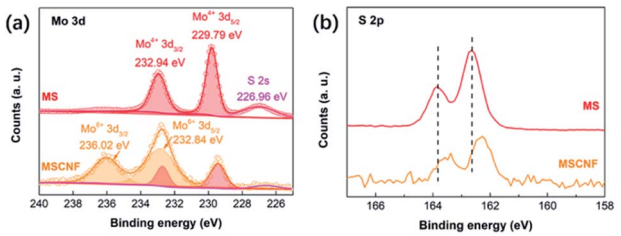

Fig. 4 XPS spectra of Mo 3d (a) and S 2p (b).

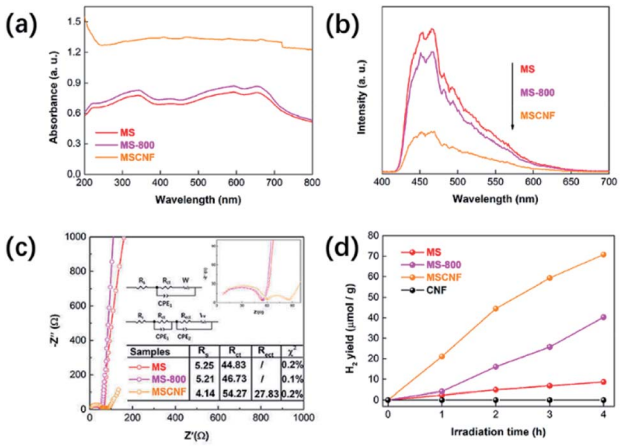

Fig. 5 (a) UV-vis diffuse reflectance spectra of the samples; (b) PL spectra of the samples; (c) Nyquist plots of the samples; and (d) temporal photocatalytic H_2 evolution of the samples.

can be ascribed to Mo^{4+}.[19] After the MS is anchored onto the surface of CNF and carbonized, the new peaks at 236.02 and 232.84 eV can be assigned to the increased Mo^{6+} and its proportion is about approximately 74% (calculated using the peak area ratio of Mo 3d),[43] indicating that the Mo atoms on the surface are oxidized during the carbonization process, which is beneficial for charge carrier transportation.[44] Based on the integrated peak areas of the Mo 3d and S 2p doublets, the S : Mo ratio decreased from 1.81 : 1 in MS to 1.58 : 1 in MSCNF, which indicates that the S atoms on the surface are also oxidized. The decrease in the peak of S 2s located at 226.96 eV further confirms the deduction.[18] In addition, the electron paramagnetic resonance spectroscopy (EPR) result (Fig. S2†) shows that no S-vacancy is generated after calcination. A shift in the S 2p peaks in the MS and MSCNF was also found (Fig. 4b), indicating that some electronic interactions and transfers occur between the MS and CNF.

Fig. 5a shows the UV-vis absorption spectra of the as-prepared MS, the MS calcined at 800 °C in nitrogen for 2 h (called MS-800), and MSCNT. As shown, the MS-800 has a stronger light absorption than that of the single MS, which can be assigned to the presence of Mo^{6+}. After the MS is deposited on the CNT, the enhanced absorption in the full spectra can be clearly observed, which is ascribed to the full spectrum absorption of the carbon nanofibers. PL is used to investigate the separation efficiency of the photo-generated carriers (Fig. 5b). Herein, the weaker PL intensity corresponds to the lower recombination.[45,46] It can be obviously seen that the intensity of MS-800 is lower than that of MS, indicating that the surface oxidation can improve the activity of the exposed edge of the MS to reduce the recombination of the photo-generated carriers effectively. The intensity of MSCNF is further reduced, which could be attributed to the fact that the electrons excited from MS would transfer to CNF quickly, avoiding a direct recombination with the corresponding holes. The results of the electrochemical impedance spectroscopy (EIS) further demonstrate the deduction (Fig. 5c). An equivalent circuit is proposed to fit the spectra. The equivalent circuit for the MS and MS-800 samples is composed of a resistor R_s (the solution resistance between the Ag/AgCl reference electrode and the working electrode) and an electrode–electrolyte interfacial charge transfer resistor R_{ct}. Obviously, compared with MS and MS-800, the MSCNF sample has an extra electron transfer resistor R_{ect}, and the resistance value is much smaller than that of MS and MS-800. This indicates that there is a charge transfer between the MoS_2 and carbon fiber, and the high conductivity of the carbon fiber can promote the separation of the photo-generated electron–hole pairs.[9,47–49] Fig. 5d displays the H_2 evolution activity of the different samples. The H_2 evolution rate of MSCNF is up to about eight times that of MS and is about two times that of MS-800. As shown in Fig. S3,† in consecutive 12 h (3 cycles) hydrogen production processes, the MSCNF sample exhibits a commendable stability. Herein, a possible photocatalytic mechanism can be deduced. The results obtained using EIS and PL indicate that the carrier migration and separation of MoS_2 shows little change before and after calcination. However, the H_2 evolution rate of MS-800 can be up to about four times that of MS, therefore the main reason for the enhanced photocatalytic performance is that the oxidation of the Mo atoms increases the active sites of MoS_2.[50] The introduction of CNF further reduces the PL intensity and improves the photocatalytic activity, indicating that CNF accelerated the carrier migration and separation efficiency owing to its high conductivity.

Conclusions

In summary, we have developed a simple method to prepare MoS_2 sheet/carbon nanofibers. The surface Mo and S atoms are oxidized by calcination in nitrogen at a high temperature, which can increase the activity of the exposed edge of MS. Herein, the introduction of CNF and increased Mo^{6+} can enhance the photo-generated charge carrier transportation to facilitate effective electron–hole pairs separation, which is beneficial for enhancing the HER performance. As a consequence, an enhanced H_2 generation was achieved in MSCNF (eight fold more than normal MoS_2). This work may provide a novel avenue for commercialization of the photocatalyst.

Conflicts of interest

There are no conflicts to declare.

Acknowledgements

This work was supported by the National Natural Science Foundation of China (Grant No. 51672249, 51802282, 11804301, 52062023 and 22066024) and the Fundamental Research Funds of Zhejiang Sci-Tech University (No. 2019Q062).

Notes and references

1 P. Taberna, J. B. Barbosa, A. Balocchi, I. Gerber, K. Urita, A. Barnabe, X. Marie and J. Chane-Ching, *Chem. Eng. J.*, 2021, **424**, 130433.
2 S. Wei, S. Chang, J. Qian and X. Xu, *Small*, 2021, **17**, 2100084.
3 W. Zhong, X. Wu, Y. Liu, X. Wang, J. Fan and H. Yu, *Appl. Catal., B*, 2021, **280**, 119455.
4 Z. Wang, H. H. Wu, Q. Li, F. Besenbacher, Y. Li, X. C. Zeng and M. Dong, *Adv. Sci.*, 2020, **7**, 1901382.
5 S. Wei, S. Ni and X. Xu, *Chin. J. Catal.*, 2018, **39**, 510–516.
6 H. Yan and H. Yang, *J. Alloys Compd.*, 2011, **509**, L26–L29.
7 L. J. Zhang, S. Li, B. K. Liu, D. J. Wang and T. F. Xie, *ACS Catal.*, 2014, **4**, 3724–3729.
8 K. Chang, Z. Mei, T. Wang, Q. Kang, S. Ouyang and J. Ye, *ACS Nano*, 2014, **8**, 7078–7087.
9 Z. Wang, X. Xiong, J. Li and M. Dong, *Mater. Today Phys.*, 2021, **16**, 100290.
10 Z. Wang, Q. Li, H. Xu, C. Dahl-Petersen, Q. Yang, D. Cheng, D. Cao, F. Besenbacher, J. V. Lauritsen and S. Helveg, *Nano Energy*, 2018, **49**, 634–643.
11 C. Pan, T. Takata, K. Kumamoto, S. S. K. Ma, K. Ueda, T. Minegishi, M. Nakabayashi, T. Matsumoto, N. Shibata and Y. Ikuhara, *J. Mater. Chem. A*, 2016, **4**, 4544–4552.
12 C. Pan, T. Takata, M. Nakabayashi, T. Matsumoto, N. Shibata, Y. Ikuhara and K. Domen, *Angew. Chem., Int. Ed.*, 2015, **54**, 2955–2959.
13 Z. Li, X. Meng and Z. Zhang, *J. Photochem. Photobiol., C*, 2018, **35**, 39–55.
14 Y.-J. Yuan, P. Wang, Z. Li, Y. Wu, W. Bai, Y. Su, J. Guan, S. Wu, J. Zhong and Z.-T. Yu, *Appl. Catal., B*, 2019, **242**, 1–8.
15 F.-J. Zhang, X. Li, X.-Y. Sun, C. Kong, W.-J. Xie, Z. Li and J. Liu, *Appl. Surf. Sci.*, 2019, **487**, 734–742.
16 S. Y. Qi, X. T. Liu, N. L. Ma and H. Y. Xu, *Chem. Phys. Lett.*, 2021, **763**, 138203.
17 Y. R. Sun, C. Xue, L. Chen, Y. K. Li, S. W. Guo, Y. L. Shen, F. Dong, G. S. Shao and P. Zhang, *Sol. RRL*, 2021, **5**, 2000722.
18 J. Ekspong, T. Sharifi, A. Shchukarev, A. Klechikov, T. Wågberg and E. Gracia-Espino, *Adv. Funct. Mater.*, 2016, **26**, 6766–6776.
19 Y. Chen, F. Su, H. Xie, R. Wang, C. Ding, J. Huang, Y. Xu and L. Ye, *Chem. Eng. J.*, 2021, **404**, 126498.
20 R. Li, L. Yang, T. Xiong, Y. Wu, L. Cao, D. Yuan and W. Zhou, *J. Power Sources*, 2017, **356**, 133–139.
21 D. Kong, H. Wang, J. J. Cha, M. Pasta, K. J. Koski, J. Yao and Y. Cui, *Nano Lett.*, 2013, **13**, 1341–1347.
22 D. Voiry, M. Salehi, R. Silva, T. Fujita, M. Chen, T. Asefa, V. B. Shenoy, G. Eda and M. Chhowalla, *Nano Lett.*, 2013, **13**, 6222–6227.
23 T. Sun, J. Wang, X. Chi, Y. Lin, Z. Chen, X. Ling, C. Qiu, Y. Xu, L. Song and W. Chen, *ACS Catal.*, 2018, **8**, 7585–7592.
24 M. Remskar, A. Mrzel, Z. Skraba, A. Jesih, M. Ceh, J. Demšar, P. Stadelmann, F. Lévy and D. Mihailovic, *Science*, 2001, **292**, 479–481.
25 H. X. Fang, H. Guo, C. G. Niu, C. Liang, D. W. Huang, N. Tang, H. Y. Liu, Y. Y. Yang and L. Li, *Chem. Eng. J.*, 2020, **402**, 126185.
26 M. Matsuoka, T. Kamegawa, R. Takeuchi and M. Anpo, *Catal. Today*, 2007, **122**, 39–45.
27 H. Jeziorowski and H. Knoezinger, *J. Phys. Chem.*, 1979, **83**, 1166–1173.
28 Y.-J. Yuan, Y. Yang, Z. Li, D. Chen, S. Wu, G. Fang, W. Bai, M. Ding, L.-X. Yang, D.-P. Cao, Z.-T. Yu and Z.-G. Zou, *ACS Appl. Energy Mater.*, 2018, **1**, 1400–1407.
29 J. Q. Pan, B. B. Wang, Z. J. Dong, C. Zhao, Z. Y. Jiang, C. S. Song, J. J. Wang, Y. Y. Zheng and C. R. Li, *Int. J. Hydrogen Energy*, 2019, **44**, 19942–19952.
30 Q. Hu, X. Liu, B. Zhu, L. Fan, X. Chai, Q. Zhang, J. Liu, C. He and Z. Lin, *Nano Energy*, 2018, **50**, 212–219.
31 Y. H. Song, Z. Mo, J. J. Fu, X. N. Zhang, X. J. She, J. J. Yuan, H. X. Chen, J. C. Qian, C. Q. Zhou, Y. S. Wu, W. S. Yang, H. M. Li and H. Xu, *Colloids Surf., A*, 2021, **617**, 126151.
32 K. E. Greenstein, M. R. Nagorzanski, B. Kelsay, E. M. Verdugo, N. V. Myung, G. F. Parkin and D. M. Cwiertny, *Environ. Sci.: Nano*, 2021, **8**, 711–722.
33 Y. K. Kim, M. Kim, S.-H. Hwang, S. K. Lim, H. Park and S. Kim, *Int. J. Hydrogen Energy*, 2015, **40**, 136–145.
34 M.-Q. Wang, C. Ye, H. Liu, M. Xu and S.-J. Bao, *Angew. Chem., Int. Ed.*, 2018, **57**, 1963–1967.
35 Y. K. Kim, S. K. Lim, H. Park, M. R. Hoffmann and S. Kim, *Appl. Catal., B*, 2016, **196**, 216–222.
36 J.-J. Li, M. Zhang, B. Weng, J. Chen and H. Jia, *J. Alloys Compd.*, 2020, 849.
37 P. Zhang, C. Shao, Z. Zhang, M. Zhang, J. Mu, Z. Guo and Y. Liu, *Nanoscale*, 2011, **3**, 3357–3363.
38 N. A. Garcia-Gomez, D. I. Garcia-Gutierrez, S. Sepulveda-Guzman and E. M. Sanchez, *J. Mater. Sci.: Mater. Electron.*, 2013, **24**, 3976–3984.

39 W. Guo, F. Zhang, C. Lin and Z. L. Wang, *Adv. Mater.*, 2012, **24**, 4761–4764.
40 Y. Gu, C. Li, J. Bai, J. Wang and T. Ma, *Vacuum*, 2016, **130**, 1–6.
41 B. Pant, H. R. Pant, N. A. M. Barakat, M. Park, K. Jeon, Y. Choi and H.-Y. Kim, *Ceram. Int.*, 2013, **39**, 7029–7035.
42 P. Bindu and S. Thomas, *J. Theor. Appl. Phys.*, 2014, **8**, 123–134.
43 Z. Chen, D. Cummins, B. N. Reinecke, E. Clark, M. K. Sunkara and T. F. Jaramillo, *Nano Lett.*, 2011, **11**, 4168–4175.
44 L. Yang, Y. Xiong, W. Guo, J. Guo, D. Gao, Y. Zhang and P. Xiao, *Electrochim. Acta*, 2017, **256**, 268–277.
45 S. Wei, S. Chang, F. Yang, Z. Fu, G. Liu and X. Xu, *Chem. Commun.*, 2021, **57**, 4412–4415.
46 S. Wei, J. Gao, P. Wu, B. Yao, H. Xu, Y. Tan, S. Liu, R. Wu, Y. Wang and L. Wang, *Ceram. Int.*, 2021, **47**, 28296–28303.
47 S. Wei, G. Zhang and X. Xu, *Appl. Catal., B*, 2018, **237**, 373–381.
48 T. Qin, Z. Wang, Y. Wang, F. Besenbacher, M. Otyepka and M. Dong, *Nano-Micro Lett.*, 2021, **13**, 1–34.
49 Y. Wang, L. Hao, Y. Zeng, X. Cao, H. Huang, J. Liu, X. Chen, S. Wei, L. Gan and P. Yang, *J. Alloys Compd.*, 2021, **886**, 161176.
50 F. Li, R. Tao, B. Cao, L. Yang and Z. Wang, *Adv. Funct. Mater.*, 2021, **31**, 2104367.